Journal of Luminescence 200 (2018) 260–264

Contents lists available at ScienceDirect

Journal of Luminescence

journal homepage: www.elsevier.com/locate/jlumin

Up-conversion mechanisms in Er^{3+}-doped fluoroindate glasses under 1550 nm excitation for enhancing photocurrent of crystalline silicon solar cell

T. Castro[a,*], D. Manzani[b], S.J.L. Ribeiro[a,*]

[a] Institute of Chemistry, São Paulo State University – UNESP, Araraquara, SP 14801-970, Brazil
[b] São Carlos Institute of Chemistry, University of São Paulo, São Carlos, SP 13566-590, Brazil

ARTICLE INFO

Keywords:
Fluoroindate glasses
Rare-earth
Solar cell
Photocurrent

ABSTRACT

In this work, Er^{3+}-containing fluoroindate glasses were synthesized by the conventional melt-quenching method varying Er^{3+} content from 0.1 to 7 mol%. The series of fluoroindate glass were investigated according to their luminescent properties. Upon excitation at 1550 nm, all glass samples showed green, red and near-infrared emissions centered at 550, 667 and 978 nm. Energy transfer upconversion (ETU) is the main mechanism responsible for the upconverted emissions and involves neighbour erbium ions. The highest near-infrared emission intensity at 1000 nm is observed for the glass sample containing 7 mol% of Er^{3+}, which was used to evaluate the photovoltaic response of monocrystalline and monofacial silicon solar cell. This approach represents a beneficial strategy to stud spectral modification in upconverter materials.

1. Introduction

Luminescent layers for solar cell (LLSC) have been extensively studied in the last decades to increase the solar photons harvesting and thereby enhancing the solar cell (SC) efficiency [1–3]. It has been demonstrated that the integration of bulk inorganic glasses on different SC, displays some advantages when comparing with the use of powder materials [4,5]. Such layers offer less preparation steps and methods, allow fast assembly and does not interfere with the electric current flowing on the semiconductor due to the uncontact with the photoanode.

Most of these layers comprises near infrared absorption and provide visible and near infrared emissions by the addition of certain types of trivalent lanthanides ions (Ln^{3+}) [6,7]. Among the Ln^{3+}, Er^{3+} has become one of the most deployed candidate for SC applications due to its energy levels that are multiples of the transition $^4I_{15/2} \rightarrow {}^4I_{13/2}$, which may be activated when excited at wavelengths from 1400 to 1580 nm [8,9]. In a resonant manner, the transitions responsible for green ($^4S_{3/2} \rightarrow {}^4I_{15/2}$), red ($^4I_{9/2} \rightarrow {}^4I_{15/2}$) and near infrared ($^4I_{11/2} \rightarrow {}^4I_{15/2}$) emissions may occur by sequential absorption of lower energy excitation photons through the energy state absorption (ESA) and energy transfer up-conversion (ETU) mechanisms [10,11]. Indeed, previous papers have been reported the energy transfer between Er^{3+}-Yb^{3+} co-doped glasses [12–14].

Crystalline silicon (c-Si) is the most traditional and employed SC, and efficiently absorbs radiation close to its bandgap of 1.12 eV [15]. In other words, photons with higher wavelength than 1100 nm loses energy by transmission and, therefore, is not useful to generate photocurrent, called sub band-gap photons [16]. An alternative to overcome this drawback is the use of Ln^{3+}-doped materials, which convert infrared radiation into visible and, in some cases, near infrared light through up-conversion (UC) mechanisms [17]. UC phenomenon consists of a sequential absorption of two or more photons by a Ln^{3+}, followed by the emission of one photon of higher energy [18,19]. Thus, these materials can increase SC photocurrent by converting absorbed low energy photons in to high-energy photons with useful wavelength for the SC [20].

Many efforts have been devoted to the study of luminescent properties of Er^{3+}/Yb^{3+} co-doped glass to increase the efficiency of SC through UC emissions [21–23]. Among the glass types, fluoroindate glasses are promising candidates due to their low phonon energy (~ 500 cm^{-1}) and large transparency window from 250 to 8000 nm, depending the chemical composition [24]. M. Rodríguez et al. reported visible and near infrared UC emissions of an Er^{3+}/Yb^{3+} co-doped fluoroindate glasses upon 1480 nm excitation and showed an improvement of the short-circuit current by the visible and infrared emissions on a monocrystalline silicon plate [25]. Balaji et al. recently reported the influence of 980 nm emission in the photocurrent of a

* Corresponding authors.
E-mail addresses: tarcio@iq.unesp.br (T. Castro), sidney@iq.unesp.br (S.J.L. Ribeiro).

https://doi.org/10.1016/j.jlumin.2018.04.028
Received 31 January 2018; Received in revised form 21 March 2018; Accepted 12 April 2018
Available online 13 April 2018

multi-crystalline silicon SC when using an Er^{3+}/Yb^{3+} co-doped fluorotellurite glass [26]. In fact, most of the works aim to study the enhancement of 980 nm emission through energy transfer between Er^{3+} and Yb^{3+}.

Although the Er^{3+}/Yb^{3+} pair is vastly used for enhancing silicon SC efficiency, this work aims to study the strictly management of Er^{3+} concentration in a low phonon energy glass to provide an efficient enhancement of SC current through UC emissions under near infrared excitation. The advantages of single Er^{3+} doped materials concerning SC applications have already been demonstrated [27–29]. In this context, we present the synthesis and evaluation of the UC mechanisms in Er^{3+}-doped fluoroindate glasses. Considering photoluminescence analysis, a detailed investigation was performed in order to understand the role of Er^{3+} in the energy transfer according to their visible and near-infrared emissions and decay time dynamics. Furthermore, we analyzed the dependence of UC emission in the enhancement of short circuit-current of a commercial silicon when excited at 1550 nm.

2. Experimental section

Doped fluoroindate glasses containing different Er^{3+} concentrations were prepared according to the molar composition rule (100-x)[40-InF_3–20ZnF_2–20SrF_2–20BaF_2]:xErF_3 varying x from 0.1 to 7 mol%. The samples were prepared by the conventional melt-quenching method in a platinum crucible tube. The raw materials In_2O_3 (Metaleurop-99.999%), ZnF_2 (Fluka-97%), SrF_2 (Alfa Aesar-99%), BaF_2 (Acros Organics-99%) and Er_2O_3 (Sigma-Aldrich-99.99%) were stoichiometrically weighted and well-mixed with an excess of ammonium bifluoride, NH_4HF_2, and then heated at 330 °C during 2 h for fluorination reaction of the oxides precursors. The melting was carried out at 850 °C during 20 min into a vertical electric furnace. The melted batches were poured out into a pre-heated mold at 240 °C, annealed for 2 h and slowly cooled to room temperature to minimize residual internal stress during the quenching process [30]. For better readability, the glass samples were labeled as IZSB-E01, IZSB-E05, IZSB-E1, IZSB-E2, IZSB-E4, IZSB-E5 and IZSB-E7.

Absorption spectra were recorded at room temperature from polished samples by using a Carry 500 Spectrophotometer (Varian) from 200 to 2000 nm with a resolution of 1 nm. The UC measurements were obtained at room temperature by using a diode laser operating at 1550 nm with 22 mW power (The Rock – NP Photonics). Visible and near infrared emission spectra were recorded at room temperature with a portable Ocean Optics (USB 2000 +) detector, sensitive from 200 to 1100 nm. The luminescence decay curves were obtained by using a Horiba Jobin Yvon fluorimeter (Fluorolog 3) equipped with a two-photomultiplier tube (PMT) for visible and near-infrared detections (Hamamatsu model H10330A) and a pulsed Xe lamp of 450 W.

As a proof of concept, the efficiency of luminescent layers was analyzed by performing photocurrent measurements in a monofacial and monocrystalline silicon solar cell (BPW-32 diode) with dimensions of 5.4 × 4.3 × 3.2 mm and sensitive area of 7.5 mm^2. For such purpose, the functional glass pieces were placed on the surface of the SC. For the photocurrent measurements, the samples were cut and polished to obtain similar dimensions of the SC, acting as encapsulating glass with 7.5 mm^2. Sample thickness of all samples was 1 mm. The sides of the samples were covered using aluminum foil in order to minimize the loss of the emitted radiation. The samples were placed on the top of the silicon diode and perpendicularly excited with a focused broadband source operating with maximum at 1550 nm. The microampere short-circuit current was recorded for all samples by using a Keithley multimeter model 2700.

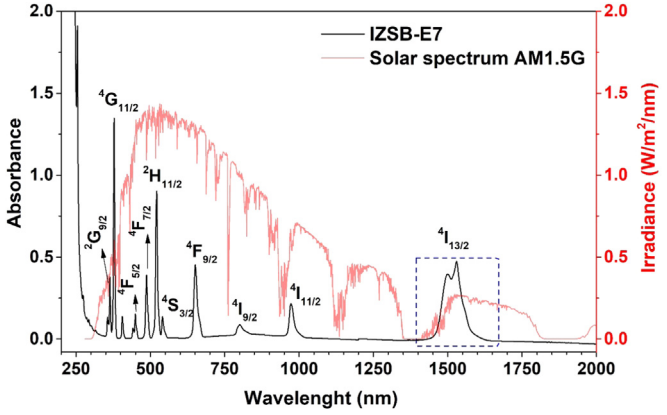

Fig. 1. Absorption spectrum of the sample IZSB-E7 (black line) and partial solar radiation spectrum AM1.5G (pink line). The dashed blue square emphasizes the overlapping between Er^{3+} absorption and solar spectrum emission over 1550 nm. (For interpretation of the references to color in this figure legend, the reader is referred to the web version of this article.).

3. Results and discussions

3.1. Photoluminescence properties

To depict the absorption spectrum of the Er^{3+}-doped fluoroindate glass, the spectrum of IZSB-E7 sample is shown in Fig. 1. Erbium ions absorption bands comprise the visible region from 380 nm to the infrared up to 1700 nm. Absorption bands are assigned to the electronic transitions from ground state level $^4I_{15/2}$, to the $^4I_{13/2}$, $^4I_{11/2}$, $^4I_{9/2}$, $^4F_{9/2}$, $^4S_{3/2}$, $^2H_{11/2}$, $^4F_{7/2}$, $^4F_{5/2}$, $^4G_{11/2}$ and $^2G_{9/2}$ excited states [31]. Below 300 nm is observed the absorption edge corresponding to the glass host band-gap energy.

At first comparison, the strongest Er^{3+} absorption at around 1500 nm matches with a spectral portion of the solar spectrum which is partially shown in Fig. 1. It is important to emphasize that wavelengths above 1100 nm are not absorbed by a silicon SC. In this sense, the feasibility to use Er^{3+} is promising for PV applications due to the possibility to increase the efficiency of traditional SC through the absorption of sub-bandgap photons and converting them into useful energy absorbed by the silicon band-gap [32]. Indeed, in Fig. 1 the dashed blue square represents the region of Er^{3+} absorption; however, the intensity of their bands does not represent a real matched area with the solar spectrum intensity, which is out of scale.

Fig. 2 shows the emission spectra of IZSB samples with the characteristic Er^{3+} emissions around 525, 550, 660, 820, 850 and 979 nm, assigned to the transitions $^2H_{11/2} \rightarrow {}^4I_{15/2}$, $^4S_{3/2} \rightarrow {}^4I_{15/2}$, $^4F_{9/2} \rightarrow {}^4I_{15/2}$, $^2H_{9/2} \rightarrow {}^4I_{9/2}$, $^4S_{3/2} \rightarrow {}^4I_{13/2}$ and $^4I_{11/2} \rightarrow {}^4I_{15/2}$, respectively. All the spectra were obtained under excitation at 1550 nm operating with 20 mW. As it is shown, the infrared emission is stronger than the green and red one for IZSB-E7. For IZSB-E01 sample, no emission was seen at naked eyes and only a very weak signal was detected. Glass samples emissions showed a strong dependence with Er^{3+} concentration, reaching a maximum intensity for IZSB-E7 sample. The dependence of UC intensity with Er^{3+} concentration is shown on the inset from the Fig. 2. The UC intensity increase significantly with Er^{3+} concentration following a linear behavior. Moreover, Fig. 2 shows the digital pictures of IZSB samples, whose present a remarkable green emission for IZSB-E7, IZSB-E4 and IZSB-E2 samples, a weak emission for IZSB-E1 sample and a very weak green spot for IZSB-E01 sample.

It is worthy to mention that 979 nm emission is one of the most desirable emissions for SC applications. This emission is equivalent to Si bandgap energy (1.1 eV); therefore, it is more capable to enhance the generation of photocurrent comparing with the green and red emissions, which present high thermalization losses [33]. In Fig. 2 is

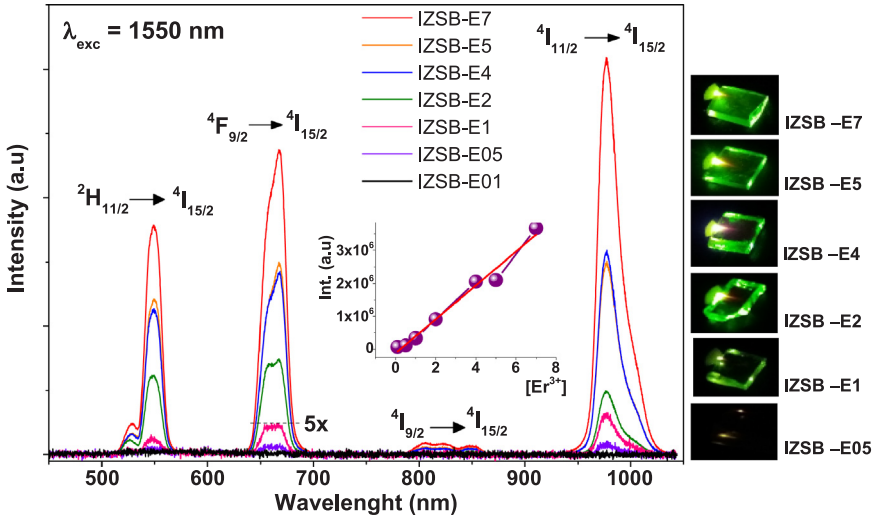

Fig. 2. Visible and near-infrared UC emission upon 1550 nm excitation and digital pictures of the samples. The sample IZSB-E01 does not exhibit emission in the visible region and the UC emission is negligible. The intensity of the samples IZSB-E1, IZSB-E05 and IZSB-E01 was multiplied by a factor of 5.

possible to see a broader emission at 979 nm than those at visible range. The emission intensity dependency with Er^{3+} concentration follows the same trend to visible emissions. The highest intensity emission is observed for IZSB-E7 sample. The mechanisms which results the visible and near infrared Er^{3+} emissions, involve two well-known mechanisms: (i) ground state absorption (GSA), and (ii) energy transfer upconversion (ETU) [34,35]. Upon excitation at 1500 nm, electrons at ground state $^4I_{15/2}$ level are excited to the first $^4I_{13/2}$ energy level through ground state absorption (GSA). After subsequent ETU process and non-radioactive decays, the $^4I_{11/2}$, $^4F_{9/2}$, $^4S_{3/2}$ and $^2H_{11/2}$ levels are populated. From the populated states mentioned above, radiative transitions take place due to the relaxation of excited electrons to the ground state through $^4I_{11/2}$, $^4F_{9/2}$, $^4S_{3/2}$, $^2H_{11/2} \rightarrow {}^4I_{15/2}$ transitions. The infrared UC emission intensity is higher than the green and red one for IZSB-E7 sample, indicating a high rate of electronic populating of the $^4I_{11/2}$ level. In fact, the Er^{3+} emissions rate is highly dependent with ion concentration, wavelength and excitation power [36–38]. For the sample IZSB-E7, we believe that an ETU process is responsible for the increase of the NIR emission, meanwhile for lower amount (0.5, 1 and 2 mol%) the red and infrared, the intensity is quite similar. A third mechanism that may takes place, is the cross relaxation (CR) due to the high concentration or erbium ions in IZSB-E7 sample. The energy difference between $^4F_{7/2} \rightarrow {}^4I_{11/2}$ and $^4I_{13/2} \rightarrow {}^4I_{15/2}$ transitions are very close in energy, thus the population of $^4I_{11/2}$ state may occur by CR, increasing the NIR emission.

For last, but not least, excited state absorption (ESA) is another process recurrently mentioned to explain the population at the emissive Er^{3+} levels. In this case, one ion is excited to its first energy level through GSA ($^4I_{15/2} \rightarrow {}^4I_{13/2}$) process. After two consecutive photon absorptions, the states $^4I_{9/2}$ and $^4S_{3/2}/{}^2H_{11/2}$ are populated. Since the energy difference between the states $^4I_{9/2}$ and $^4I_{11/2}$ is 2.300 cm^{-1}, it requires more than 4 photons (fluoroindate phonon energy of 500 cm^{-1}) to relax non-radiatively, therefore, a three-sequential photon absorption is favored. However, ESA is a process of one single ion and its efficiency is strongly suppressed by the weak absorption induced by parity-forbidden intra-4f transition within 4f orbitals [39]. The number of photons necessary to populate the emitter states are presented elsewhere [7]. The number of photons involved in the emissions at 980 nm, 550 nm and 660 nm are 2, 3 and 4, respectively. Fig. 3 shows a scheme of the partial energy diagram of Er^{3+}. GSA, ESA and ETU processes are summarized as well as radiative transitions (green and red arrows) and non-radiative transitions (dashed arrows).

Decay curves of IZSB samples for green, red and NIR emissions are depicted in Fig. 4 and the values of the experimental decay curves are

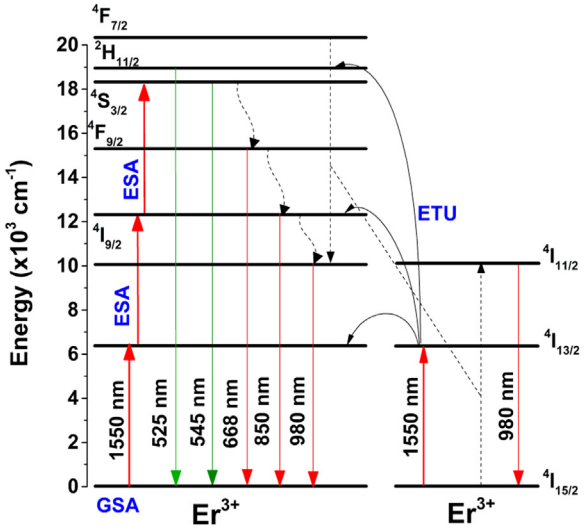

Fig. 3. Schematic energy level diagram for Er^{3+}-doped fluoroindate glass under excitation at 1550 nm.

listed in Table 1. The samples were excited at 521 nm and emissions were fixed at 550, 668 and 980 nm. The curves were fitted by a mono-exponential function and the life times are shown in Fig. 4. The interaction between Er^{3+}-Er^{3+} plays an important role since it depends of Er^{3+} concentration, and the smaller distance is straight responsible by the decreasing of lifetime for all the radiative emissions. The longer decay time for $^4H_{11/2}$ and $^4S_{9/2}$ levels comparing with the $^4I_{11/2}$ state, indicates that these first two state are more associated with non-radiative transitions, meanwhile, the population of $^4I_{11/2}$ state is favored, leading to the highest intensity in the PL measurements.

3.2. Photocurrent analysis

To evaluate the viability to use upconverting materials coupled into solar cells, we performed photocurrent measurements by placing the glass samples under a commercial and monofacial silicon SC. The samples were perpendicularly excited at 1550 nm. To minimize the UC radiation losses, the four glass edges were covered with aluminum foil. The experimental setup is shown in Fig. 5.

In agreement with the UC intensities, for IZSB-E7 sample the Si SC exhibits the highest short-circuit current value, 210 μA, meanwhile a

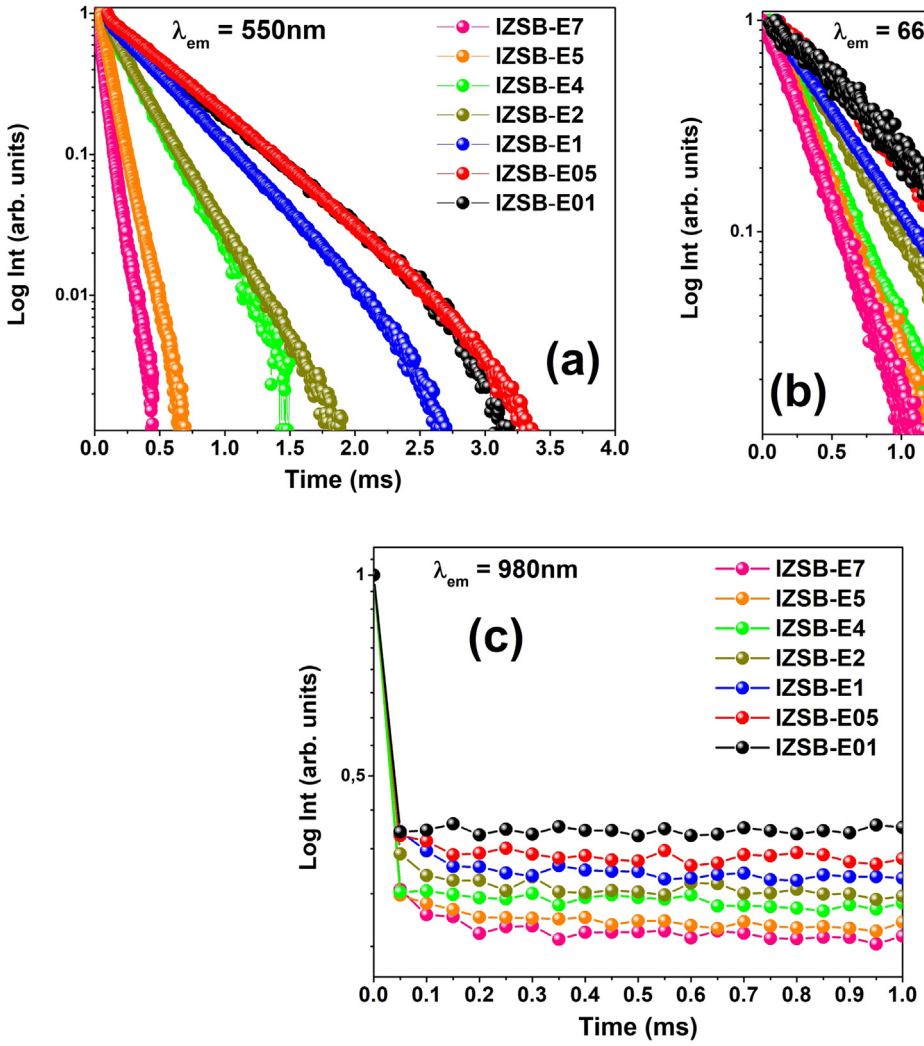

Fig. 4. Decay time for green, red and near-infrared emission under excitation at 521 nm, figure (a), (b) and (c), respectively. (For interpretation of the references to color in this figure legend, the reader is referred to the web version of this article.).

Table 1
Experimental decay time values for the samples under excitation at 521 nm.

Sample	Lifetime (ms)		
	550 nm	668 nm	980 nm
IZSB-E01	0.563	0.678	0.503
IZSB-E05	0.579	0.580	0.461
IZSB-E1	0.447	0.449	0.304
IZSB-E2	0.238	0.384	0.296
IZSB-E4	0.090	0.302	0.275
IZSB-E5	0.067	0.295	0.125
IZSB-E7	0.060	0.270	0.103

very weak signal is observed for IZSB-E01 and IZSB-E05 that are 0.40 and 3.23 μA, respectively. Under direct illumination or using an un-doped sample, the short-circuit current was negligible.

It is important to emphasize when the samples are placed on the top of the SC, a substantial fraction of the emitted radiation is lost through the top of the uncovered face (surface where the laser beam is focused). In the last two decades, several studies presented the concept of UC materials using a luminescent layer located at the rear face of a bifacial solar cell, instead of at on the top. Besides, a mirror located beneath the luminescent layer, would help to collect the UC emission at the rear surface. Therefore, an UC material placed at the front surface of a solar

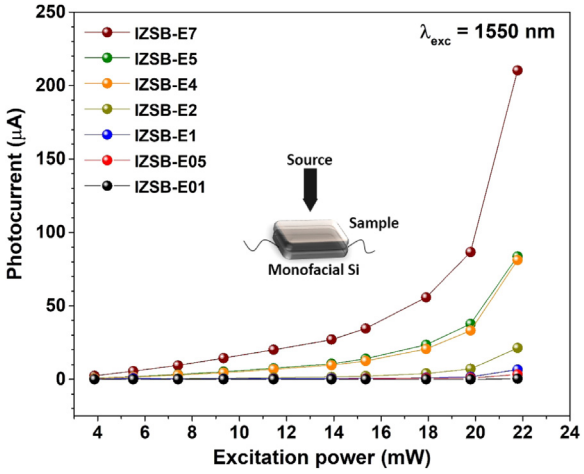

Fig. 5. Photocurrent analysis of the samples as a function of the power source excitation. Experimental setup for the photocurrent analysis (inset figure). The samples were place on the top of a Si SC and excited with a perpendicular beam at 1550 nm. All the measurements were performed in a dark room.

cell is acceptable as a proof of concept, but nor for commercial purposes.

Unfortunately, it is a hard task to compare the presented results with those already presented in the literature. Most of them reports short-circuit current in small pieces of glass comparing to the active SC area. Moreover, take into account some parameters like glass thickness, refractive index, impurities, mono and/or polycrystalline diode and monochromatic excitation; we may expect different photocurrent values. In fact, a figure of merit for this kind of analysis is needed and would be necessary to compare the SC performance among different glass systems.

4. Conclusions

In conclusion, we prepare fluoroindate glasses with different Er^{3+} concentration as UC material for enhancement of monocrystalline solar cell photocurrent. All Er^{3+} compositions allowed us to obtain green, red and near infrared emission through UC mechanisms. The near-infrared emission at 980 nm, which match with the Si bandgap, increases when the concentration is 7 mol% of Er^{3+} and decreases above this concentration. According to the short circuit-current measurements, we have verified the influence of UC emissions in the generation of extra current by placing the samples under a monocrystalline Si solar cell. The excitation at 1550 nm with 22 mW provided a maximum of 200 μA to the SC showing the highest UC emission.

Acknowledgments

The authors are thankful for the support of the Brazilian agencies FAPESP, Capes and CNPq.

References

[1] F. Lahoz, C. Perez-Rodríguez, S.E. Hernandez, I.R. Martín, V. Lavín, U.R. Rodrıguez-Mendoza, Sol. Energy Mater. Sol. Cells 95 (2011) 1671–1677.
[2] B.S. Richards, Sol. Energy Mater. Sol. Cells 90 (2006) 2329–2337.
[3] A. Shalav, B.S. Richards, T. Trupke, K.W. Krämer, H.U. Güdel, Appl. Phys. Lett. 86 (2005) 013505.
[4] Pei Song, Chaomin Zhang, Pengfei Zhu, J. Alloy. Compd. 678 (2016) 65–69.
[5] Nikhil Chander, Atif F. Khan, Vamsi K. Komarala, Santa Chawla, Viresh Dutta, Prog. Photovolt.: Res. Appl. 24 (2016) 692–703.
[6] J. Feenstra, I.F. Six, M.A.H. Asselbergs, R.H. van Leest, J. de Wild, A. Meijerink, R.E.I. Schropp, A.E. Rowanb, J.J. Schermera, Phys. Chem. Chem. Phys. 17 (2015) 11234–11243.
[7] H. Rodríguez-Rodríguez, M.H. Imanieh, F. Lahoz, I.R. Martín, Sol. Energy Mater. Sol. Cells 144 (2016) 29–32.
[8] Yannan Qian, Rui Wang, Biao Wang, Baofu Zhang, Senpei Gao, RSC Adv. 4 (2014) 6652–6656.
[9] Pierre Gigart, François Auzel, Jean-Claude Guillaume, Khaled Zahraman, J. Appl. Phys. 35 (1996) 4401–4402.
[10] H. Dong, L. Sun, C. Yan, Chem. Soc. Rev. 44 (2015) 1608–1634.
[11] I.R. Martın, P. Velez, V.D. Rodriguez, U.R. Rodrıguez-Mendoza, V. Lavın, Spectrochim. Acta Part A 55 (1999) 935–940.
[12] Fang Yang, Chao Liu, Dong Wei, Yongsheng Chen, Jingxiao Lu, Shi-e. Yang, Opt. Mater. 36 (2014) 1040–1043.
[13] Z.Q. Li, X.D. Li, Q.Q. Liu, X.H. Chen, Z. Sun, C. Liu, X.J. Ye, S.M. Huang, Nanotechnology 23 (2012) 025402.
[14] Guo-Bin Shan, Hassane Assaaoudi, George P. Demopoulos, ACS Appl. Mater. Interfaces 9 (2011) 3239–3243.
[15] Olfa Maalej, Julien Merigeon, Brigitte Boulard, Mihaela Girtan, Opt. Mater. 60 (2016) 235–239.
[16] Jan Christoph Goldschmidt, Stefan Fischer, Adv. Opt. Mater. 3 (2015) 510–535.
[17] R. Reisfeld, Z. Naturforsch. B 69b (2014) 131–140.
[18] A. Shalav, B.S. Richards, M.A. Green, Sol. Energy Mater. Sol. Cells 91 (2007) 829–842.
[19] Auzel François, Chem. Rev. 104 (1) (2004) 139–174.
[20] Sandra F.H. Correia, Verônica de Zea, Bermudez, Sidney J.L. Ribeiro, Paulo S. André, Rute A.S. Ferreira, Luís D. Carlos, J. Mater. Chem. A 2 (2014) 5580–5596.
[21] J. de Wild, A. Meijerink, J.K. Rath, W.G.J.H.M. van Sark, R.E.I. Schropp, Sol. Energy Mater. Sol. Cells 94 (2010) 1919–1922.
[22] Nannan Yao, Jinzhao Huang, Ke Fu, Xiaolong Deng, Meng Ding, RSC Adv. 6 (2016) 11880–11887.
[23] Guo-Bin Shan, George P. Demopoulos, Adv. Mater. 22 (2010) 4373–4377.
[24] L.J. Borrero-González, G. Galleani, D. Manzani, L.A.O. Nunes, S.J.L. Ribeiro, Opt. Mater. 35 (2013) 2085–2089.
[25] M.A. Hernández-Rodríguez, M.H. Imanieh, L.L. Martín, I.R. Martín, Sol. Energy Mater. Sol. Cells 116 (2013) 171–175.
[26] Sathravada Balaji, Debarati Ghosh, Kaushik Biswas, Amarnath R. Allu, Gaurav Gupta, Kalyandurg Annapurna, J. Lumin. 187 (2017) 441–448.
[27] A. Shalav, B.S. Richards, T. Trupke, K.W. Krämer, H.U. Güdel, Appl. Phys. Lett. 86 (2005) 013505.
[28] Jiangli Wang, Jihuai Wu, Jianming Lin, Miaoliang Huang, Chem. Sus. Chem. 5 (2012) 1307–1312.
[29] F. Pellé, S. Ivanova, J.F. Guillemoles, EPJ Photovolt. 2 (2011) 20601.
[30] D. Manzani, D. Paboeuf, S.J.L. Ribeiro, P. Goldner, F. Bretenaker, Opt. Mater. 35 (2013) 383–386.
[31] M.C. Pujol, M. Rico, C. Zaldo, R. Solé, Appl. Phys. B 68 (1999) 187–197.
[32] Bryan M. van der Ende, Linda Aartsa, Andries Meijerink, Phys. Chem. Chem. Phys. 11 (2009) 11081–11095.
[33] B.S. Richards, Sol. Energy Mater. Sol. Cells 90 (2006) 1189–1207.
[34] T. Catunda, L.A.O. Nunes, A. Florez, Y. Messaddeq, M.A. Aegerter, Phys. Rev. B 53 (1996) 6065–6070.
[35] K. Venkata Krishnaiah, J. Marques-Hueso, K. Suresh, G. Venkataiah, B.S. Richards, C.K. Jayasankar, J. Lumin. 169 (2016) 270–276.
[36] Fiorenzo Vetrone, John-Christopher Boyer, John A. Capobianco, Adolfo Speghini, Marco Bettinelli, Chem. Mater. 15 (2003) 2737–2743.
[37] Haizhou Lu, William P. Gillin, Ignacio Hernández, Phys. Chem. Chem. Phys. 16 (2014) 20957–20963.
[38] G.A. Kumar, M. Pokhrel, D.K. Sardar, Mater. Lett. 68 (2012) 395–398.
[39] K. Venkata Krishnaiah, P. Venkatalakshmamma, Ch Basavapoornima, I.R. Martín, K. Soler-Carracedo, M.A. Hernandez-Rodríguez, V. Venkatramu, C.K. Jayasankar, Mater. Chem. Phys. 199 (2017) 67–72.